Measurement of the axial vector mass in neutrino-Oxygen interactions

Richard Gran, Eun Ju Jeon,* and K2K collaboration

High Energy Accelerator Research Organization (KEK)

Tsukuba 305-0801, Japan

Replace these with the full author list later.

(Dated: August 1, 2005)

Abstract

The weak nucleon axial-vector form factor is determined using neutrino interaction data from the K2K Scintillating Fiber detector in the neutrino beam at KEK. More than 12,000 events are analyzed, of which half are charged-current quasi-elastic interactions $\nu_\mu n \rightarrow \mu^- p$ occurring primarily in Oxygen nuclei. By assuming the form factor is approximately a dipole with one parameter, the axial vector mass M_A, we fit to the shape of the distribution of the square of the momentum transfer from the nucleon to the nucleus. Our best fit result for $M_A = 1.16$ GeV $\pm$ 0.12 stat. $\pm$ 0.03 syst. This analysis includes updated vector form factors from recent electron scattering experiments and a discussion of the effects of the nucleon momentum on the shape of the fitted distributions.

PACS numbers: 13.15.+g; 23.40.Bw; 25.30.Pt

*Now at Seoul National University

I. INTRODUCTION

The structure of the nucleon, as measured both by electrons and neutrinos, has been a subject of experimental study for decades. The discovery of neutrino oscillation and the availability of high precision electron scattering measurements have renewed interest in the study of neutrino interactions on nuclei. Neutrinos offer unique information about the nucleon and the nucleus. There are many experimental neutrino programs now running, under construction, or being planned for the near future, all of which use nuclear targets such as Oxygen, Carbon, Aluminum, Argon, or Iron. Likewise, there has been significant progress in the calculation of cross sections, backgrounds, and nuclear corrections.

In this study we analyze distributions of the square of the four-momentum transfer $Q^2 = -q^2 = -(p_\mu - p_\nu)^2$ for neutrino-Oxygen interactions, where p_μ and p_ν are the momenta for the outgoing muon and incident neutrino. Using data from the Scintillating Fiber (SciFi) detector in the K2K neutrino beam we fit for the value of the axial vector mass M_A, the single parameter in the axial vector dipole form factor for quasi-elastic interactions. This is the first such measurement for Oxygen nuclei, and we include a discussion of the effects of the Oxygen nucleus and nucleon momentum distribution on the shape of the Q^2 distribution.

II. CROSS SECTIONS

A. Quasi-elastic cross section

The differential cross section $d\sigma/dq^2$ for neutrino quasi-elastic scattering ($\nu_\mu \mathrm{n} \rightarrow \mu^- \mathrm{p}$) is described in terms of the vector, axial-vector, and pseudo-scalar form factors. The differential cross section is written as:

$$\frac{d\sigma^{\nu(\bar{\nu})}}{dq^2} = \frac{M^2 G_F^2 \cos^2\theta_c}{8\pi E_\nu^2} \times \left[A(q^2) \mp B(q^2)\frac{s-u}{M^2} + C(q^2)\frac{(s-u)^2}{M^4} \right] \quad (1)$$

where, s and u are Mandelstam variables, (s-u) = 4ME_ν - q^2 - m^2, m is the outgoing lepton mass, M is the target nucleon mass, and E_ν is the neutrino energy[1]. $A(q^2)$, $B(q^2)$,

and $C(q^2)$ are:

$$\begin{aligned}
A(q^2) &= \frac{m^2-q^2}{4M^2}\Big[(4-\frac{q^2}{M^2})|F_A|^2 \\
&\quad -(4+\frac{q^2}{M^2})|F_V^1|^2 - \frac{q^2}{M^2}|\xi F_V^2|^2(1+\frac{q^2}{4M^2}) \\
&\quad -\frac{4q^2F_V^1\xi F_V^2}{M^2} - \frac{m^2}{M^2}((F_V^1+\xi F_V^2)^2+|F_A|^2)\Big], \\
B(q^2) &= \frac{q^2}{M^2}(F_A(F_V^1+\xi F_V^2)), \\
C(q^2) &= \frac{1}{4}\left(|F_A|^2+|F_V^1|^2-\frac{q^2}{4M^2}|\xi F_V^2|^2\right). \qquad (2)
\end{aligned}$$

In these expressions, the pseudo-scalar form factor F_P is negligible for muon neutrino scattering away from the muon production threshold and is not included. $F_V^1(q^2)$ and $F_V^2(q^2)$ are the Dirac electromagnetic isovector form factor and the Pauli electromagnetic isovector form factor, respectively. These formulas also assume the conserved vector current (CVC) hypothesis, which allows us to write F_V^1 and F_V^2 in terms of the well measured Sachs form factors G_E^P, G_E^N, G_M^P, and G_M^N:

$$\begin{aligned}
F_V^1(q^2) &= (1-\frac{q^2}{4M^2})^{-1}\Big[(G_E^P(q^2)-G_E^N(q^2)) \\
&\quad -\frac{q^2}{4M^2}(G_M^P(q^2)-G_M^N(q^2))\Big], \\
\xi F_V^2(q^2) &= (1-\frac{q^2}{4M^2})^{-1}\left[(G_M^P(q^2)-G_M^N(q^2))\right. \\
&\quad \left.-(G_E^P(q^2)-G_E^N(q^2))\right]. \qquad (3)
\end{aligned}$$

In this paper we use the updated measurements of the Sachs form factors from [2, 3]. These new form factors have a significant effect on the extraction of F_A, compared to the previous dipole approximations. For the range of Q^2 of interest in this experiment, the updated values differ from the old form factors by up to $\pm$ 10%. We present results with both the new and the old form factors in this paper.

We approximate the axial vector form factor F_A as a dipole

$$F_A(q^2) = -\frac{1.267}{\left(1-(q^2/M_A^2)\right)^2}, \qquad (4)$$

which has a single free parameter, the axial vector mass. Previous studies show that this approximation is reasonable [4–6], given the statistical and systematic limitations of neutrino scattering experiments.

B. Other cross sections

For this analysis, approximately half of the data comes from non quasi-elastic interactions, mostly single pion events from the production and decay of the N and Δ baryon resonances within the nucleus. This background is described by the NEUT Monte Carlo [7] used by the K2K and Super-Kamiokande experiments. The resonance single pion events are from the model of Rein and Sehgal[8]. Deep inelastic scattering is from GRV94[9] with a correction described by Bodek and Yang[10]. This analysis takes the coherent pion cross section to be zero following [11], but we include a discussion of results with coherent pion interactions as in Rein and Sehgal[12] with modifications following Marteau[13, 14], which has been used in the previous K2K publications.

C. Nuclear Effects

Equation 1 is the differential cross section for the *free* nucleon, and must be modified to account for the effects of a nucleon bound in a nucleus. In the SciFi detector, the fiducial mass fractions are 0.723 H_2O, 0.205 Al, 0.072 HC, with an error of ± 0.004. Our neutrino interaction Monte Carlo treats the entire fiducial mass as if it was made of H_2O; for targets other than a proton in Hydrogen, we use a Fermi gas model with $k_f = 225$ GeV/c for the nucleon momentum and an effective binding energy of 27 MeV, which is appropriate for Oxygen. The primary effect of this nucleon momentum distribution on the quasi-elastic events is an overall suppression of $\sim$2% for the entire Q^2 distribution and a significant suppression at low Q^2 due to Pauli blocking. The Fermi gas model is also applied to the non quasi-elastic interactions.

In addition to cross section effects, there are final-state interactions. The nucleus will cause reinteraction or absorption of secondary pions and recoil protons. This will affect the observed distribution of the number of tracks. The resulting μ^- is also affected by the Coulomb interaction as it leaves the nucleus, losing approximately 3 MeV. The above nuclear effects are discussed quantitatively in the results section and in Fig. 7.

III. EXPERIMENT

The KEK to Kamioka (K2K) experiment is a long baseline neutrino oscillation measurement in which a beam of neutrinos is sent from the KEK accelerator in Tsukuba, Japan, through a set of near neutrino detectors 300 meters from the target, after which they travel 250 km to the underground Super-Kamiokande detector[15–17]. The analysis in this paper considers only neutrino interactions detected in the Scintillating Fiber (SciFi) detector, one of the near detectors.

The wide-band neutrino beam at KEK is produced when 12 GeV protons hit an aluminum target. A magnetic horn focuses positively charged pions into a 200 meter long decay pipe, where they decay to μ^+ and ν_μ. The μ^+ are absorbed by approximately 100 meters of earth between the beam dump and the near detector hall. The resulting neutrino energy is between 0.3 and 5 GeV and peaks at 1.2 GeV. The contamination in this beam includes 1.3% ν_e and 0.5% anti-ν_μ. There are also a small number of muons which need to be vetoed; they come from in-time muon generation in the rock and upstream material in the detector hall and a negligible number of muons surviving from the beam dump and decay pipe. These are rejected by an upstream scintillator veto system. Cosmic rays are rejected by a beam timing requirement, and are also negligible.

The near detector hall of the K2K experiment contains several detectors. The first one in the beam is the 1 kiloton water Cerenkov detector. This study uses data from the SciFi detector, which is the next one in the beam and is described in detail below. Surrounding SciFi are upstream and downstream veto counters, and after 2002 there are top and side veto counters as well. Following that is the location of a lead glass detector. The lead glass detector was removed in 2002 and in its place was a prototype for a plastic scintillator (SciBar) detector. Then in 2003, the full SciBar detector [18] was installed, though data from this last running period is not used in the present analysis. Finally, there is a muon range detector (MRD) [19] which is used to estimate the momentum of the muons from charged current neutrino interactions. These detector arrangements are summarized in Fig. 1.

The SciFi detector [20, 21] consists of scintillating fiber tracking layers between aluminum tanks filled with water. A schematic diagram is included in Fig. 1. There are a total of twenty 240 cm wide tracking layers, each of which consists of fibers oriented to give the location in the horizontal and vertical direction. These fibers are glued, one layer on each side, to

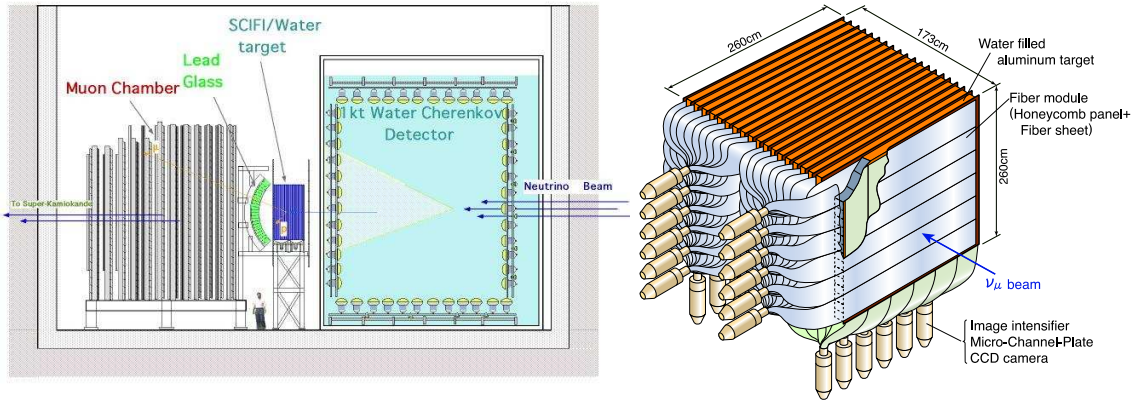

FIG. 1: The arrangement of the near neutrino detectors at KEK (left) and a schematic diagram of the SciFi detector.

a honeycomb panel which is 260 cm square. The distance between two tracking layers is 9 cm. Between the first and the twentieth layer are nineteen layers of aluminum tanks whose walls are 0.18 cm thick with an interior thickness 6 cm filled with water.

The scintillating fibers have a diameter of 0.7 mm and are read out by coupling two image intensifier tubes and a CCD camera. The image intensifier preserves the position information of the original photo-electron. At the final stage, the light is recorded by a CCD camera. To reconstruct which fibers were hit, a one-to-one correspondence between the fibers and the position of pixels on the CCD camera is obtained from periodic calibration using an electro-luminescent plate.

The SciFi detector has upstream and downstream veto detectors made from plastic scintillator which are read out by photo-multiplier tubes. For the neutrino events in this analysis, we require that muon tracks match one or more hits in the downstream veto as they exit SciFi and have no corresponding hits in the upstream veto counters. Since 2002 there are also top and side veto counters to facilitate contained event studies; these are not used for the charged-current events with exiting muons in this analysis.

Tracks are reconstructed in the horizontal and vertical projections separately and then matched. For the primary muon track from charged-current events, we require that it start in the SciFi fiducial volume and extend to the muon range detector. The efficiency for reconstructing muon tracks with hits in three SciFi tracking layers is $\sim$70%, and rises to nearly 100% for tracks that penetrate five or more layers. Second (and third...) tracks are

required to produce hits in at least three SciFi layers, but there is no restriction on the maximum length. When two tracks reach the MRD, the longest, most penetrating track is assumed to be the muon. Approximately 2% of these longest tracks are not the muon track, and another 0.5% of events were from neutral current interactions which had no muon at all, which we have estimated using the MC.

The fiducial mass used for this analysis is 5.6 tons, corresponding to an interaction vertex at least 10 cm in from the edge of the detectors and occurring between the second and eighteenth tracking layers. When this is combined with the upstream veto efficiency, the contamination from muons from the beam, the earth, the water Cerenkov detector, and also from cosmic rays is negligible.

Prior to 2002, all muons from SciFi are required to pass through the lead glass detector. On average, they deposit around 0.4 GeV of energy there. After 2002, muons traveling through the SciBar prototype lose around 0.23 GeV of energy. Muons traveling through many layers in SciFi deposit up to 0.3 GeV of energy.

The Muon Range Detector is made of alternating layers of drift tubes and iron plates; the first detection layer is upstream of the first piece of iron. The first four layers have a thickness equivalent to about 0.15 GeV of energy loss, and the remaining layers are twice as thick. The muon momentum can then be estimated by calculating its range from the interaction vertex. The requirement that muons do not exit the MRD results in a maximum muon momentum of 3.5 GeV/c.

A. Data samples

The data for this analysis are obtained from three running periods between November 1999 and June 2003. We refer to the first two as the "K2K-I" period; muons from neutrino interactions in SciFi pass through a lead glass detector on their way to the MRD. For these data, we accept muons which penetrate as little as one MRD detection layer, which corresponds to a muon momentum threshold of 400 MeV/c. The third running period is called "K2K-IIa" and has the prototype for the plastic scintillator detector SciBar [18] in place of the Lead Glass. For K2K-IIa, we require that the muons produce hits in the first *two* layers of the MRD, which gives a threshold of 550 MeV/c.

This analysis uses only one-track and two-track events. The 3% of events with three or

more reconstructed tracks are discarded. For one-track events, the recoil proton or a pion is absent or below threshold. The requirement of three layers for the second track corresponds to a threshold of 600 MeV/c proton momentum and 200 MeV/c pion momentum.

In the case of two-track events, we separate quasi-elastic from non-quasi-elastic events. For QE interactions, the measurement of the muon momentum and angle is sufficient information to predict the angle of the recoil proton. If the measured second track agrees with this prediction within 25°, it is likely a QE event. If it disagrees, then it becomes a part of the non-QE sample. The value for this cut is chosen to give good separation between these samples. In this way we have an enhanced sample which is 60% QE, and another sample which is 15% QE, estimated from our Monte Carlo. The one-track sample is also 60% QE. The total number of events in each sample is given in Tab. I.

	K2K-I		K2K-IIa	
q^2 $(GeV/c)^2$	$Q^2 > 0.0$	$Q^2 > 0.2$	$Q^2 > 0.0$	$Q^2 > 0.2$
1 track	5933	2864	3623	1659
2 track QE	740	657	451	388
2 track nonQE	1441	789	893	478
Total	8114	4310	4967	2525

TABLE I: Number of events in three event samples and two data periods for the SciFi detector. The columns that include only events with $Q^2_{rec} > 0.2$ (GeV/c)^2 are used for this M_A measurement.

B. Basic p_μ and θ_μ distributions

An example of the muon momentum distribution for the K2K-I data along with the Monte Carlo prediction is shown in Fig. 2. The MC prediction uses the results from the near detector neutrino energy spectrum analysis [17].

We observe a deficit of events whose muon is at angles near the direction of the beam compared to our Monte Carlo; this is also discussed in [17]. The discrepancy is observed in all K2K near detectors, including SciFi, and is presumed to be from some aspect of the neutrino interaction model. The analysis of data from the SciBar detector [11] indicates that much of this deficit is because there is too much coherent pion production in the Monte

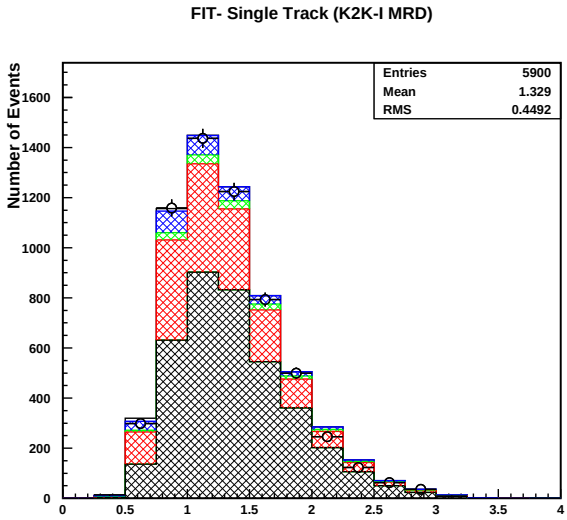

FIG. 2: Pmu distribution. THIS FIGURE NEEDS TO BE RE-MADE SHOWING ONLY THE QE FRACTION. [RIK will remake this with all the data (not just 1-track) showing the QE fraction and using the spectrum fit and no coherent pion for the MC.]

Carlo. The data are consistent with zero charged-current coherent pion. Examples of the disagreement from SciFi data are shown in Fig. 3, with and without coherent pion.

The axial-vector analysis is a fit to the Q^2_{rec} distribution of the data, and the small angles with respect to the beam for which we observe the above discrepancy correspond to $Q^2_{rec} < 0.1$ (GeV/c)^2. The discrepancy between our data and Monte Carlo is as much as 20% at the lowest Q^2. In addition to the observed discrepancy, the uncertainty in the cross section models at low Q^2 are larger than at moderate and high Q^2. This region is not included in the analysis; we include events with $Q^2_{rec} > 0.2$ (GeV/c)^2. The total number of events actually used is also shown in Tab. I. This cut is the same as the one used in the previous analyses of neutrino interactions[4–6].

IV. ANALYSIS

A. Calculating Q^2 and E_ν

The kinematics of the muon, the longest track in our events, are sufficient to estimate the energy of the neutrino $E_{\nu rec}$ and the square of the momentum transfer Q^2_{rec}, if the interaction

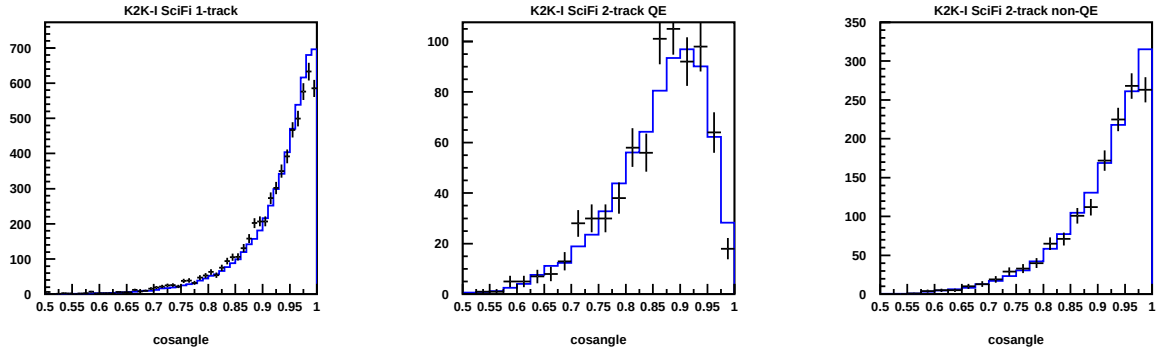

FIG. 3: Example of the discrepancy between data and Monte Carlo for muons in the forward direction. This is the distribution of the cosine of the angle between the muon and the beam for the 1-track, 2-track QE, and 2-track non-QE samples. [RIK will remake this with coherent pion and without coherent pion MC prediction, and with QE fraction.

is quasi-elastic.

$$E_{\nu rec} = \frac{(m_N + \epsilon_B)E_\mu - (2m_N\epsilon_B + \epsilon_B^2 + m_\mu^2)/2}{m_N + \epsilon_B - E_\mu + p_\mu \cos\theta_\mu}, \tag{5}$$

$$Q^2_{rec} = -q^2 = -2E_\nu(E_\mu - p_\mu \cos\theta_\mu) + m_\mu^2. \tag{6}$$

Here, E_μ and p_μ are the energy and momentum of the muon, determined from the range, θ_μ is the angle determined from the hits in the SciFi detector. Note that E_ν appears in the expression for Q^2_{rec}. The quantity ϵ_B = -27 MeV for Oxygen is the effective binding energy parameter from the Fermi gas model. The masses m_N and m_μ are for the nucleon and the muon. The resolution for E_μ is 0.12 GeV, due mainly to the MRD segmentation, though the mean of the distribution is accurate to 1%. The resolution for θ_μ is about 1 degree, but there is a tail to this distribution for events with significant activity around the vertex. [Make sure of this statement.] The resulting value for E_ν resolution is 0.16 GeV and the resolution for Q^2_{rec} is 0.05 (GeV/c)^2 also with a tail coming from the measured angle. Finally, this formula assumes that the target neutron inside the nucleus is at rest, ignoring the nucleon momentum distribution for the event reconstruction. Fluctuations due to Fermi motion are about half of those due to detector and reconstruction effects, and contribute only a small

amount to the reconstructed energy resolution.

It is important to note that these formulas are used for all events even though half the interactions are not quasi-elastic, because we do not identify the interaction mode on an event-by-event basis, nor is our beam at a fixed energy. The reconstructed E_ν and Q^2 are systematically off for these non quasi-elastic events: $E_{\nu rec}$ is low by $\sim$0.4 GeV and Q^2_{rec} is low by $\sim$0.05 (GeV/c)^2. However, all events are treated the same way, both data and Monte Carlo. Thus, the comparison of data and MC in the fit is valid, but the distributions of the reconstructed values are affected by the non quasi-elastic fraction.

B. Fit procedure

After calculating $E_{\nu rec}$ and Q^2_{rec} for each event, the data are binned in five $E_{\nu rec}$ bins: 0.5 to 1.0, 1.0 to 1.5, 1.5 to 2.0, 2.0 to 2.5, and greater than 2.5 GeV. The data are divided into Q^2 bins each of width 0.1 (GeV/c)^2. To ensure there are at least five events in each bin, the smaller number of events at higher Q^2 are combined into a single bin.

The expectation for the number of the events in each bin is computed for different values of the axial-vector mass and some systematic error parameters. We perform a maximum likelihood fit to the data by minimizing the negative of the logarithm of the likelihood which is based on Poisson statistics for each bin. In our case we use the modified form given in the Review of Particle Physics [22]

$$-2\ln\lambda(\theta) = 2\sum_{i=1}^{N}[\nu_i(\theta) - n_i + n_i\ln(n_i/\nu_i(\theta))]$$

in which $\nu_i(\theta)$ and n_i are the predicted and observed values in the i-th bin for some values of the parameters θ. Unlike the ordinary Poisson likelihood, the minimum of this function follows a chi-square distribution and can be used to estimate the goodness of the fit.

The expectation for each reconstructed E_ν and Q^2 bin is computed as follows:

$$\begin{aligned}\nu(E,q^2) \;=\; A\,\Big[&\mathrm{flux}(E)\times d\sigma/dq^2(E,q^2,M_A)\times R(E,q^2)\\ &+ B\times \mathrm{nonQE}(E,q^2)\Big]\times\Phi(E).\end{aligned} \tag{7}$$

The quasi-elastic cross section $d\sigma/dq^2$ is for free neutrons and the reweighting function R accounts for the effects of the nucleus. The shape of the non-QE distribution is taken directly from our Monte Carlo which already includes the nuclear effects. The parameter B

= nonQE/QE ratio is a free parameter in the fit. Because of the separation of the two-track QE and non-QE samples, the nonQE/QE ratio will constrain the background and giving a fit for the QE axial vector form factor. The distribution flux(E) includes the detailed shape of our neutrino energy flux within each energy bin and is taken from the beam MC. Five free parameters $\Phi(E)$, one for each neutrino energy region, reweight this predicted flux and account for neutrino flux uncertainty.

The formula above leaves out one aspect of the calculation in order to make the method clear. The quasi-elastic cross section must still be modified to account for the detector acceptance and resolution. This is done with a migration matrix $M(E_{true}, q^2_{true} \rightarrow n_{track}, E_{rec}, q^2_{rec})$, where n_{track} refers to the one-track, two-track QE, and two-track non-QE samples. This matrix is computed directly from the Monte Carlo. This result is then applied to the calculated cross section to determine the number of QE events in each reconstructed E_ν and Q^2 bin.

$$N_{QE}(n_{track}, E_{rec}, q^2_{rec}) = \sum_{Etrue,q^2true}^{\text{allbins}} [N_{QE}(E_{true}, q^2_{true}, M_A) \times M(E_{true}, q^2_{true} \rightarrow N_{track}, E_{rec}, q^2_{rec})].$$

The value $N_{QE}(E_{true}, q^2_{true}, M_A)$ is the first product in brackets in Eq. 7. Again, the shape of the non-QE background is taken directly from the Monte Carlo and reweighted only by the nonQE/QE ratio and the flux in each neutrino energy bin, and a calculation such as the one above is not necessary because that information is already included.

The prediction for the neutrino flux in each energy bin is based on our beam Monte Carlo which uses a Sanford-Wang formula fit to data from pion production experiments. This is described with detailed references in [15]. There is significant uncertainty in these predictions, up to 20% at higher energies, so the flux parameters $\Phi(E)$ in the M_A fit are used to reweight the baseline prediction. In this way we are fitting the shape of the Q^2_{rec} distribution separately *in each energy region*. This ensures that the axial mass measurement is not significantly biased by the normalization in any one energy bin.

V. RESULTS

We fit a large ensemble of E_ν and Q^2 distributions: two data sets K2K-I and K2K-IIa, each with one-track, two-track QE, and two-track non-QE subsamples, a total of 242 bins. The Monte Carlo predictions for these data sets are computed separately and use a

MC sample that is 15 times larger than the data. The free parameters for the flux at each energy are common to both subsamples, as is the non-QE/QE ratio and proton rescattering.

The result of the combined fit is $M_A = 1.16 \pm 0.12$ GeV. The chisquare value for this fit is 260 for 230 degrees of freedom. The Q^2 distributions for the data and the best fit M_A are shown in Fig. 4, with all five energy regions combined.

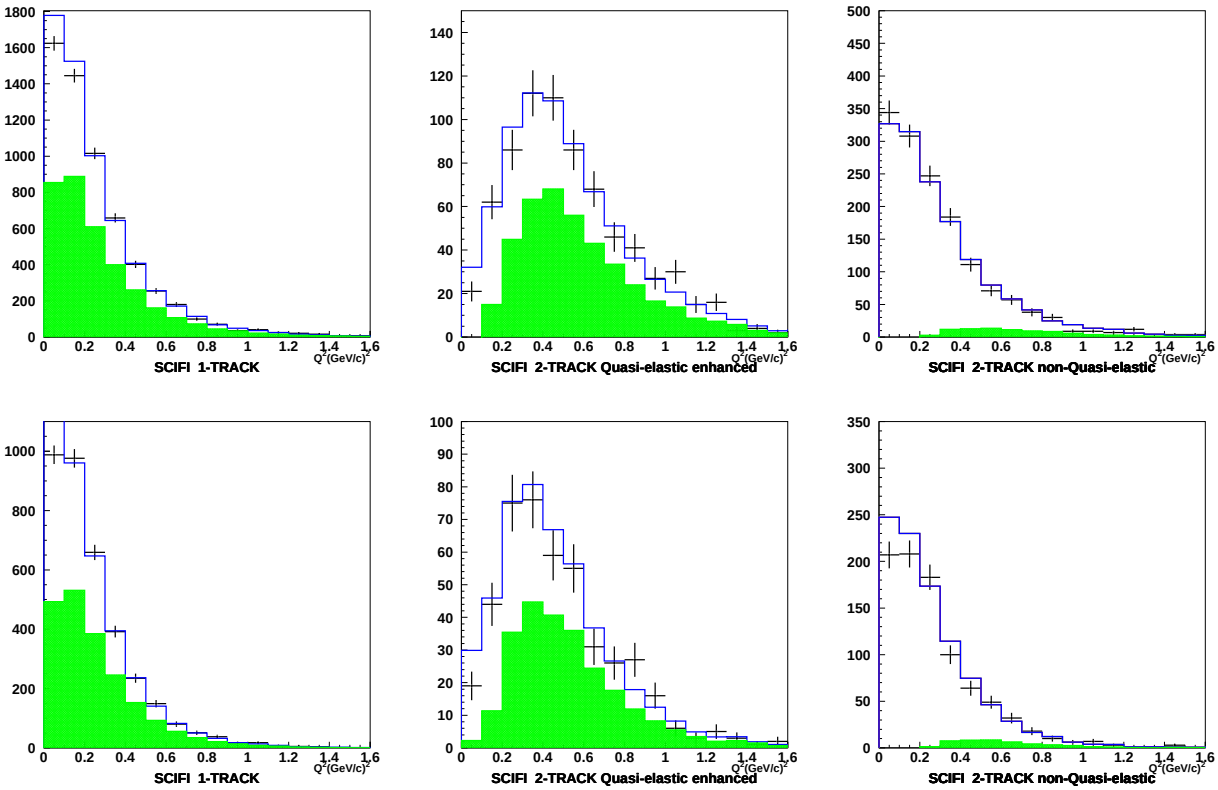

FIG. 4: The data and the best fit Q^2 distributions for K2K-1 data (top) and K2K-IIa data (bottom) for the 1-track, 2-track QE enhanced, and 2-track non-QE enhanced samples. The shaded region shows the QE fraction of each sample, estimated from the MC. The contribution from each energy region is summed for each plot.

A. Consistency checks

The K2K-I and K2K-IIa samples are also fit separately. We obtain the values 1.12 ± 0.12 and 1.25 ± 0.18 respectively. Another check is to consider the fit values for the Q^2 distribution *at each energy*, shown in Fig. 5. This uses the best fit values for the flux for

all energies except the one being tested while the chisquare, and therefore the shape fit, is computed only for the energy bins in question. This is necessary because the significant migration from true energy (where the flux parameter is applied) to reconstructed energy used in the fit. There are different systematic effects, and this result should not be considered a measurement, but rather a consistency test. However results for each energy are also consistent with the combined result.

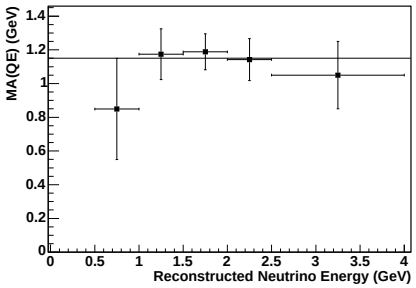

FIG. 5: Fit values obtained separately from the shape of the Q^2 distribution for each neutrino energy. The horizontal line indicates the combined best fit value.

A final test for consistency is to consider the effect of the low Q^2 cut. In Fig. 6, when no cut is applied (and no coherent pion), the fit value is $M_A = 1.24 \pm 0.12$, where the statistical error is less, but a large systematic error of $\pm$ 0.07 is assigned due to uncertainty in the amount of Pauli Blocking. If coherent pion events are included, the fit value rises to 1.34. In contrast, as the cut is moved to higher Q^2, the result remains consistent, indicating that the dipole approximation is reasonable. At Q^2 of 0.2, adding coherent pion pushes M_A only 0.01 GeV/c^2 higher, while at yet higher Q^2 there is no effect.

B. Systematic uncertainties

The largest contributions to the systematic error are the uncertainty in the muon momentum scale and the uncertainty in the flux for each energy region. Other, smaller contributions include the shape of the non-QE background and the non-QE/QE ratio. A final, interesting source of uncertainty comes from nuclear effects, though it contributes only a small amount to this analysis. The main errors are summarized in Tab. II and described below.

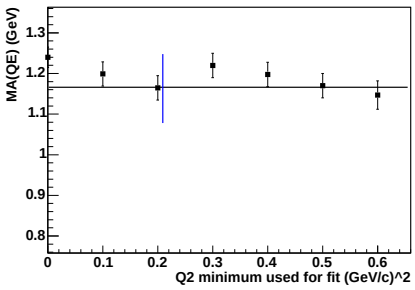

FIG. 6: Fit values obtained for different values of the low Q^2 cut. The horizontal line is the combined best fit.

Sources of uncertainty	Error in MA
Relative Flux and normalization	0.08
Energy Scale	0.07
MA 1-π	0.03
nonQE/QE	0.03
Statistics	0.03
Total	0.12

TABLE II: The calculation of the total error. Errors smaller than 0.03 are not included in the total. The total value takes into account the correlations among those errors that are parameters in the M_A fit; the others are added to that total in quadrature.

1. Flux for each energy region

A significant uncertainty arises because the relative neutrino flux for each energy region and two overall normalization parameters (one for each data set) are unconstrained parameters in the fit. The relative flux for incident neutrinos in the region from 1.0 GeV to 1.5 GeV is set to 1.0 and the other energy regions are free parameters. The shape of the spectrum is the same for both K2K-I and K2K-IIa, but they are allowed to have different relative normalizations, though the fit returns nearly the same result for both. [Rik says obviously he should reprogram this to be a single free parameter. This will be checked.] In this way we are fitting the shape the Q^2 distribution in each energy region separately, regardless of the errors in the incident neutrino flux.

The overall normalization contributes more to the error than the uncertain relative normalization. Also, the overall normalization is highly correlated with M_A because M_A affects both the normalization and the shape of the QE cross-section. Finally, different combinations of MA and normalization will give a reasonable chisquare, and the error due to this parameter, more than the others, would be reduced with increased data statistics, even with no further constraints.

We do have a constraint on the relative flux for each energy region from the neutrino oscillation measurement [17]. This measurement is done using data from all the near detectors, not just SciFi. This information is not completely independent of this analysis because it shares some of the same data set, but a different analysis technique, and several other data sets from the other near detectors. We get a consistent result $M_A = 1.13 \pm 0.12$ when this constraint is used.

2. Muon momentum scale

The muon momentum appears directly, and indirectly via E_ν, in the calculation of the value of Q^2 for each event. The uncertain absolute scale for this momentum, as modeled in the detector Monte Carlo, will cause the MC prediction for the shape of the Q^2 distribution to be more or less compressed. For these data, a $\pm$ 1% error in the momentum scale gives a $\mp$ 0.05 error in the fit value for M_A. Approximately $\mp$ 0.01 of this error can be attributed to an energy binning effect, the other $\mp$ 0.04 is from the calculation of the reconstructed Q^2 itself.

Because the muon momentum is measured using its range in the detector, the uncertainty for the overall momentum may come from any of the pieces of the detector. In this analysis, we model this uncertainty by assigning it to two pieces. The first is the uncertainty in the density of the lead-glass detector and therefore the energy loss experienced by the muon passing through it. The second piece is a scaling factor for part of the muon momentum calculated from the range in the MRD detector. For both pieces, we determine the central value of the momentum shift and the error from the neutrino data. This is not done within the M_A analysis, rather it is done with the spectrum fit analysis [17], and then applied here.

We have used a Monte Carlo simulation to study the potential effect of a 5% uncertainty in the lead glass density, which is the result of a beam test, and made a reweighting table

that modifies the MC p_μ and θ_μ distribution. This uncertainty would give rise to a 2% error in the total momentum for a typical K2K-I event. In the spectrum analysis used for the oscillation measurement, this is a parameter in the fit and good agreement with the data is found with a value that is 0.98 ± 0.013 times the density obtained from the beam test; the neutrino data provides the stronger constraint. This central value is used in the M_A analysis.

Likewise, we measure a shift in the muon momentum scale for in the Muon Range Detector (MRD) of 0.976 ± 0.007 using the spectrum fit procedure. When the K2K-I and K2K-IIa data are fit separately, we obtain a consistent result for this parameter, despite the presence of the lead glass detector in the former. This is assigned as an error for the MRD portion of the muon range, but it actually arises from a combination of factors including the material assay for the MRD and SciFi (about 1%), the simulation of muon energy loss in GEANT [23] (about 1%) and the intrinsic muon momentum from the neutrino interaction MC (about 0.5%). Again, we find the neutrino data produces a good central value and a tighter constraint than taking the individual errors in quadrature. Though these errors actually come from all portions of the muon track, we find no significant difference in the analysis if this factor is applied to the whole track momentum, instead of the MRD portion only.

Because the M_A fit and the spectrum fit use the same neutrino data, it is possible that the uncertain value for M_A itself is affecting the fit values for the MRD muon momentum scale when that value is obtained from the spectrum fit. Our default Monte Carlo assumes $M_A = 1.1$ GeV. An uncertainty in this value of ± 0.20 GeV corresponds to an error of ± 0.01 or in the fit value of the momentum scale. This is taken as an additional uncertainty when this parameter is used to determine M_A. Also, there is a correlation between the lead-glass density error and the MRD momentum error. When all of these effects are combined, the resulting error in M_A is ± 0.07.

3. nonQE/QE ratio

The nonQE/QE scaling ratio is also a free parameter in the axial-mass fit. There is no constraint on this parameter for this analysis, though other estimates find that it is uncertain by 5 to 10% [17]. This parameter accounts for uncertainties in the relative normalization of

the non-QE and QE parts, including not just the relative uncertainty in the cross sections for different processes, but also the fact that changing the QE-MA also changes the size of the QE cross section. By itself the nonQE/QE parameter contributes approximately 0.03 to the total systematic uncertainty in M_A. The fit value nonQE/QE = 1.38 ± 0.17 is relative to our default neutrino interaction Monte Carlo, meaning the best fit is found when the nonQE events are scaled up by 38%.

4. Non quasi-elastic background shape

Single pion events from the production and decay of the Δ and other resonances in the nucleus are the largest background to the QE samples in this analysis. These events are described by a calculation that includes a similar axial mass parameter which affects the shape of the Q^2 distribution. If the value used to model the single pion background is different, that will affect the fit value obtained for the quasi-elastic events. Our calculation takes $M_A^{1\pi} = 1.1 \pm 0.1$ GeV. This contributes an uncertainty of ± 0.03 to result for M_A^{QE}.

Other contributions to the nonQE background are deep inelastic scattering and coherent pion production. For the former, we have evaluated the uncertainty by removing the Bodek-Yang correction, and find no effect. We also consider the case where charged-current coherent pion events are produced which increases the fit value by 0.10 when we fit the entire Q^2 range, but has only +0.01 effect for the $Q^2 > 0.2$ analysis.

5. Nuclear effects

Another interesting source of uncertainty are the effects of the nucleus on the cross section and the Q^2 distribution, primarily from the nucleon momentum distribution. The effects are small relative to the other uncertainties described above, but will be of interest for future experiments and as models of neutrino-nucleus interactions become more sophisticated. We present a description of these effects for the Fermi Gas model, in this case from the calculation in [24, 25]. The three effects are described below and summarized in Fig. 7. It is the ratio in this figure that is the basis for $R(E,Q^2)$ in Eq. 7.

The main uncertainty is the amount of Pauli Blocking that should be applied both to the quasi-elastic and also the single pion background. This is one possible contribution to the

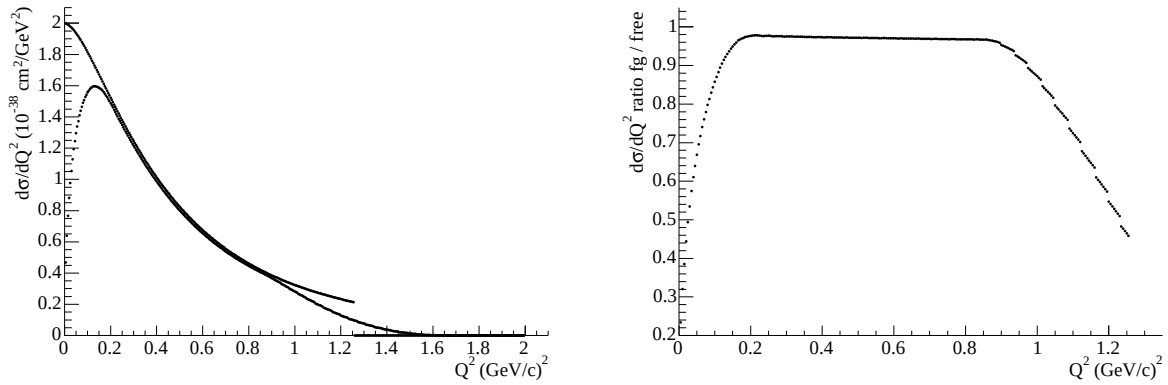

FIG. 7: Effect of the nucleon momentum on the shape of the Q^2 distribution. The comparison is between the free nucleon and a Fermi gas model. The effect of Pauli blocking is seen at low Q^2, the tail of the momentum distribution at high Q^2, an overall suppression, and a slight change in the slope in the middle region. The calculated quasi-elastic cross sections for 1.0 GeV neutrinos on Oxygen are on the left, and the ratio (Fermi gas)/ (free neutron).

discrepancy at low Q^2 described earlier. Within the context of the Fermi gas model, this can be estimated by assuming a different k_f: 215 and 235 in addition to the default value of 225 GeV/c. The effects of this uncertainty do not appear with the $Q^2 > 0.2$ requirement used in this analysis, but are as much as 5% at the lowest Q^2.

At upper end of the Q^2 distribution, the quasi-elasitic cross section has a kinematic cut off. The momentum distribution in a nucleus smears this step, giving a tail to the distribution. These high Q^2 interactions produce muons that do not reach the MRD because they are at high angle or their momentum is too low, so this has no effect on the present analysis.

The momentum distribution will modify the shape of the Q^2 distribution through the middle region between the two effects described in the preceeding paragraphs. The slope of the middle region in the second plot in Fig. 7 is approximately 0.017 $(\mathrm{GeV/c})^{-2}$. There is also an overall suppression of the cross section of 2%. The resulting uncertainty in M_A is ± 0.01, negligible compared to the other uncertainties in this analysis, and the comparison of the Fermi gas model with the free nucleon case overestimates this uncertainty.

A final uncertainty from the nuclear model is the nucleon interaction energy. For our Fermi gas model, this takes the form of an effective binding energy 27 $\pm$ 3 MeV, and is the energy given up to the recoil proton from the nucleus. This affects the outgoing muon

momentum and would contribute ± 0.02 error to M_A, but this is naturally included by the free energy scale parameter in this analysis.

These uncertainties are also used to estimate the effect of the 20.5% Aluminum that makes up the fiducial mass. The neutrino-Aluminum interactions are taken to have the same cross section per nucleon and the same kinematics as for Oxygen. A higher k_f appropriate for Aluminum only has an effect in the Pauli blocked region and the increased effective binding energy has an effect equivalent to a shift in p_μ of about 3 MeV for this fraction of the events, and thus is negligible for the whole sample.

C. Effect of the new form factors

The basic method used to measure the axial vector mass here is the same as for previous measurements, but since that time there have been improved measurements for the shape of the vector form factors from electron scattering experiments. Our results are extracted using these updated parameterizations, but in order to allow comparison with the previous results, we have repeated the analysis with the same modified dipole approximations used by [4–6] who follow Olsson *et al.* [26]. We find that these old parameterizations produce a value that is 1.20, roughly 0.04 higher. When only a pure dipole is used, the fit value rises again to 1.23 MeV.

Our results assume a parameterization of the vector form factors according to Bosted [2]. We have evaluated one other parameterization [3] and found the M_A result differs by only 0.01 GeV. This is true even considering the discrepancy between the polarization transfer measurement and the Rosenbluth separation measurement. For our values, we use the parameterization of G_E^N given by [27].

D. Comparison with other experiments

This is the first measurment of the axial vector mass using neutrino interactions with Oxygen targets, but there have been many previous measurements with a variety of other target nuclei. The following experiments have hundreds or thousands of events from neutrino or anti-neutrinos with energies of a few GeV. The systematic errors they report are dominated by uncertainties in the neutrino flux, calculation of nuclear effects, and subtraction of

Experiment	Target	Method	MA	Error	comment
ANL [6]	D	12' Bubble Chamber	1.00	± 0.05	
FNAL [5]	D	15' Bubble Chamber	1.05	+0.12 - 0.16	
BNL [4]	D	7' Bubble Chamber	1.07	+0.040 -0.045	
BNL [28]	Fe	Segmented Tracker	1.05	± 0.20	
CERN [29]	CF_3Br	GGM Bubble Chamber	0.94	± 0.17	
CERN [30]	CF_3Br, C_3H_8	GGM Bubble Chamber	0.94	± 0.05	
BNL [31]	HC, Al	Segmented Tracker	1.06	± 0.05	elastic scattering
BNL [32]	HC, Al	Segmented Tracker	1.09	± 0.04	(ν-bar)
SKAT [33]	CF_3Cl	Bubble Chamber	1.05	± 0.14	(ν)
SKAT [33]	CF_3Cl	Bubble Chamber	0.79	± 0.20	(ν-bar)
K2K SciFi	H_2O, Al	Segmented Tracker	1.23	± 0.12	dipole form factors

TABLE III: Results from other experiments. Where separate values are given for M_A extracted from the shape of $d\sigma/dQ^2$ only, that is the value included in this table. All the data are for the neutrino quasi-elastic reaction (ν n $\rightarrow \mu^-$ p) except for two which also took data with anti-neutrino (ν-bar p $\rightarrow \mu^+$ n), one of which studied neutral current (elastic) scattering, noted in the table. For better comparison with other experiments, this result is the one analyzed with dipole vector form factors.

non-quasielastic backgrounds.

One problem with comparing the results in Tab. III is that the older analyses used not only different assumptions about the vector form factors, but also different backgrounds and other physical constants such as $F_A(q^2{=}0)$ The results given here are the published results, however the authors of [3] have made some effort to reproduce and then update all of the analysis assumptions for a selection of these experiments.

VI. CONCLUSION

We have made the first measurement of axial vector form factor using neutrino interactions on an Oxygen target. We find that a dipole parameterization with an axial vector mass

$M_A = 1.16 \pm 0.12$ GeV/c^2 gives the best agreement with the data. This analysis includes the updated (non-dipole) vector form factors obtained from electron scattering experiments. In order to better compare with previous experiments, an alternate result using only pure dipole vector form factors is $M_A = 1.23 \pm 0.12$ GeV/c^2. We have also studied the details of the nucleon momentum distribution for Oxygen on this analysis and find only a small effect on the shape of the Q^2 distribution for $Q^2 > 0.2$.

Acknowledgments

Acknowledgments not yet written.

---

[1] C. L. Smith, Phys. Lett. C **3C** (1972).

[2] P. E. Bosted, Phys. Rev. C **51**, 409 (1995).

[3] H. Budd, A. Bodek, and J. Arrington, hep-ex/0308005 to appear in Nucl. Phys. B Proc. Supp. (2002).

[4] T. Kitagaki et al., Phys. Rev. D **42**, 1331 (1990).

[5] T. Kitagaki et al., Phys. Rev. D **28**, 436 (1983).

[6] K. Miller et al., Phys. Rev. D **26**, 537 (1982).

[7] Y. Hayato, Nucl. Phys. B Proc. Supp. **112**, 171 (2002).

[8] D. Rein and L. Seghal, Ann. Phys. **133**, 79 (1981).

[9] M. Gluck, E. Reya, and A. Vogt, Z. Phys. C **67**, 433 (1995).

[10] A. Bodek and U. K. Yang, Nucl. Phys. B Proc. Supp. **112**, 70 (2002).

[11] M. Hasegawa et al., Submitted to Phys. Rev. Lett. (2005), hep-ex/0506008.

[12] D. Rein and L. Seghal, Nucl. Phys. B **223**, 29 (1983).

[13] J. Marteau, Eur. Phys. J. A **5**, 183 (1999).

[14] J. Marteau, J. Delorme, and M. Ericson, Nucl. Instrum. Methods A **451**, 76 (2000).

[15] S. H. Ahn et al., Phys. Lett. B **511**, 178 (2001).

[16] M. H. Ahn et al., Physical Review Letters **90**, 041801 (2003).

[17] E. Aliu et al., Phys. Rev. Lett. **94**, 081802 (2005).

[18] K. Nitta et al., Nucl. Instrum. Methods A **535**, 147 (2004).

[19] K2K MRD Group, T. Ishii, et al., Nucl. Instrum. Methods A **482**, 244 (2002).

[20] A. Suzuki et al., Nucl. Instrum. Methods A **453**, 165 (2000).

[21] B. J. Kim et al., Nucl. Instrum. Methods A **497**, 450 (2003).

[22] S. Eidelman et al., Phys. Lett. B **592** (2004), URL `http://pdg.lbl.gov`.

[23] R. Brun et al., CERN DD/EE/84-1 (1987).

[24] H. Nakamura and R. Seki, Nucl. Phys. B Proc. Supp. **112** (2002).

[25] H. Nakamura and R. Seki, Nucl. Phys. B Proc. Supp. (2002), proc. NuInt02, Irvine, in press.

[26] M. G. Olsson, E. T. Osypowski, and E. H. Monsay, Phys. Rev. D **17**, 2938 (1978).

[27] S. Galster et al., Nucl. Phys. B **32**, 221 (1971).

[28] R. Kustom et al., Phys. Rev. Lett. **22**, 1014 (1969).

[29] S. Boneti et al., Nuovo Cimento A **38**, 260 (1977).

[30] N. Armenise et al., Nucl. Phys. B **152**, 365 (1979).

[31] L. Ahrens et al., Phys. Rev. D **35**, 785 (1987).

[32] L. Ahrens et al., Phys. Lett. B **202**, 284 (1988).

[33] J. Brunner et al., Z. Phys. C **45**, 551 (1990).